Anisotropic migration velocity analysis: Application to a data set from West Africa

Debashish Sarkar and Ilya Tsvankin
Center for Wave Phenomena, Department of Geophysics, Colorado School of Mines, Golden, CO 80401-1887, USA

ABSTRACT

Although it is widely recognized that anisotropy can have a significant influence on the focusing and positioning of migrated reflection events, conventional imaging methods still operate with isotropic velocity fields. Here, we present an application of a migration velocity analysis (MVA) algorithm designed for factorized $v(x,z)$ VTI (transversely isotropic with a vertical symmetry axis) media to an offshore data set from West Africa. By approximating the subsurface with factorized VTI blocks, it is possible to decouple the spatial variations in the vertical velocity from the anisotropic parameters with minimal *a priori* information.

Since our method accounts for lateral velocity variation, it produces more accurate estimates of the anisotropic parameters than those previously obtained with time-domain techniques. The values of the anellipticity parameter η found for the massive shales exceed 0.2, which confirms that ignoring anisotropy in the study area can lead to substantial imaging distortions, such as misstacking and mispositioning of dipping events. While some of these distortions can be removed by using anisotropic time processing, further marked improvement in image quality is achieved by prestack depth migration with the estimated factorized VTI model. In particular, many fault planes, including antithetic faults in the shallow part of the section, are better focused by the depth-migration algorithm and appear more continuous. Anisotropic depth migration also facilitates structural interpretation by eliminating false dips at the bottom of the section and improving the images of a number of gently dipping features.

One of the main difficulties in anisotropic MVA is the need to use *a priori* information for constraining the vertical velocity. In this case study, we successfully reconstructed the time-depth curve from reflection data by assuming that the vertical velocity is a continuous function of depth and estimating the vertical and lateral velocity gradients in each factorized block. If the subsurface contains strong boundaries with known jumps in velocity, this information can be incorporated into our MVA algorithm.

Key words: transverse isotropy, factorized media, velocity analysis, prestack migration, field data, P-waves

1 INTRODUCTION

Since most subsurface formations are both heterogeneous and anisotropic, building physically realistic velocity models from reflection data remains a highly challenging problem. Conventional velocity-analysis methods, which range from those employing simple analytic functions (e.g., Faust, 1951, 1953; Gardner et al., 1974) to sophisticated tomographic schemes (e.g., Stork, 1988; Liu, 1997; Meng, 1999; Chauris and Noble, 2001), are designed to account for smooth spatial velocity variations but still ignore anisotropy. Their application often

causes anisotropy-induced misties in time-depth conversion, undercorrection of nonhyperbolic moveout and misfocusing of dipping events (Tsvankin, 2001). In contrast, most existing anisotropic parameter-estimation techniques (e.g., Alkhalifah and Tsvankin, 1995; Han et al., 2000; Grechka et al., 2002) do not properly handle lateral heterogeneity, which may result in imaging of reflectors with wrong dips and poor focusing of events.

Migration algorithms suitable for imaging data from heterogeneous media of relatively simple symmetry (e.g., transversely isotropic) are readily available today. Therefore, the main difficulty is not in the imaging step, but in reconstructing a sufficiently accurate spatially varying, anisotropic velocity field. Nonuniqueness in velocity analysis arises from the tradeoffs between the velocity gradients, shapes of the reflecting interfaces, and anisotropic parameters. Some of these tradeoffs, such as those between the velocity field and reflector shapes, cannot be resolved without *a priori* information, even for isotropic media.

In particular, velocity analysis in heterogeneous, anisotropic media is compounded by the interplay between anisotropy and spatial velocity variations. For example, reflection traveltimes from a diffractor in a vertically heterogeneous isotropic medium are fully equivalent to the traveltimes from a diffractor in a homogeneous transversely isotropic medium with a vertical axis of symmetry (VTI). Therefore, it is critically important to represent the subsurface with the simplest possible model that (1) allows for anisotropy and adequately describes realistic velocity variations; (2) permits full understanding of the inherent ambiguities; and (3) requires minimal *a priori* information to resolve the relevant parameters.

Such a model for P-wave imaging in the presence of transverse isotropy was suggested by Sarkar and Tsvankin (2003; hereafter referred to as Paper I) who approximated the subsurface by a factorized $v(x,z)$ VTI medium with constant gradients in the vertical velocity. The Thomsen anisotropic parameters ϵ and δ in factorized media are constant, while the P-wave vertical velocity is described by $V_{P0}(x,z) = V_{P0} + k_x x + k_z z$, where V_{P0} is the velocity at the origin of the coordinate system ($x = 0, z = 0$), and k_z and k_x are the vertical and horizontal velocity gradients, respectively.

In addition to being the simplest VTI model with both vertical and lateral velocity variations, the factorized $v(x,z)$ VTI medium also allows for a simple analytic understanding of the ambiguities in parameter estimation. In Paper I, we showed that P-wave reflection moveout constrains only four combinations of the five medium parameters V_{P0}, k_x, k_z, ϵ, and δ:
(1) the normal-moveout (NMO) velocity at the surface $V_{\rm nmo} = V_{P0}\sqrt{1+2\delta}$;
(2) the vertical gradient k_z;
(3) the combination $\hat{k}_x = k_x\sqrt{1+2\delta}$ of the lateral gradient k_x and δ; and
(4) the Alkhalifah-Tsvankin (1995) anellipticity parameter $\eta \equiv (\epsilon - \delta)/(1+2\delta)$.
Estimation of the Thomsen parameters V_{P0}, k_x, ϵ, and δ requires minimal *a priori* information, such as knowledge of the vertical velocity at a single point in the medium.

Sarkar and Tsvankin (2004), hereafter referred to as Paper II, proposed a migration velocity analysis (MVA) algorithm to invert for the effective (moveout) parameters $V_{\rm nmo}$, k_z, $\hat{k}_x$, and η. To separate the influence of anisotropy from that of vertical heterogeneity, it is necessary to use image gathers along two reflectors sufficiently separated in depth. The residual moveout of events in image gathers is evaluated by a semblance operator (Taner and Koehler, 1969) that accounts for the nonhyperbolic (long-spread) moveout needed to constrain the anellipticity parameter η. The variance of the migrated depths is then minimized by iteratively solving a system of linear equations for the medium parameters. The algorithm assumes V_{P0} to be known at one point in each factorized layer and searches for k_z, k_x, ϵ, and δ in each layer.

In Paper II, the MVA algorithm is implemented in the layer-stripping mode, wherein the model is divided into factorized VTI layers or blocks, and the medium parameters are estimated one factorized layer at a time. In each layer, velocity analysis is performed through an iterative two-step procedure that includes Kirchhoff prestack depth migration followed by an update of the medium parameters. The iterations are stopped when events in image gathers associated with two reflectors in each factorized layer are sufficiently flat. As illustrated in Appendix A, the piecewise factorized model with a linear velocity variation in each block usually provides an adequate approximation for nonlinear velocity functions.

Here, the algorithm of Paper II is applied to a data set acquired by Chevron Overseas Petroleum Co. in offshore West Africa. The two seismic lines analyzed in this paper were previously processed by Alkhalifah et al. (1996) and Alkhalifah (1996, 1997) using time-domain velocity analysis based on the inversion of dip moveout (DMO) and of the nonhyperbolic moveout of subhorizontal events. Both inversion techniques, described in detail by Tsvankin (2001, chapter 7), were able to detect substantial anisotropy in massive shale formations and estimate the parameter η as a function of the vertical reflection time. Time migration for the reconstructed vertically heterogeneous VTI model succeeded in imaging dipping events (fault planes) that were misfocused by conventional algorithms. Also, the VTI processing improved the image of some gently dipping features by properly correcting for nonhyperbolic moveout (Alkhalifah et al., 1996; Alkhalifah, 1996, 1997) .

Since the previous studies were limited to time-domain processing, they did not account for lateral heterogeneity in either parameter estimation or migra-

tion. Application of the factorized $v(x, z)$ model here yields more accurate, laterally varying anisotropic velocity fields and greatly improved imaging of several important structural features.

2 BRIEF OVERVIEW OF THE GEOLOGICAL HISTORY

The geology of the area (offshore Angola) is largely governed by tectonic rifting that occurred around the early Cretaceous. The major tectono-stratigraphic units in the order they were formed are (Brice et al., 1982):
(1) Prerift with gentle tectonism;
(2) synrift I with strong tectonism;
(3) synrift II with moderate tectonism;
(4) postrift with gentle tectonism; and
(5) regional subsidence with major tilting.
The available seismic sections contain only the subsidence and postrift phases schematically shown in Figure 1.

The regional subsidence phase, which dates back to the Oligocene and Miocene times, is characterized by a rapidly deposited regressive sequence, turbidites, shaly clastics, and high-pressure shale. Reflectors within this unit are weak and discontinuous, and show extensive cut-and-fill patterns. The ubiquitous presence of shales makes the subsidence unit strongly anisotropic, which is well documented in the literature (Ball, 1995; Alkhalifah et al., 1996). The thickness of this unit increases away from the shore, and at places can reach 6 km.

The early Tertiary postrift deposition includes marine clastics and carbonates, nonmarine red beds, and transgressive sequences. This unit is less anisotropic than the subsudence layer and increases in thickness toward the shore, where it can be up to 2-km thick. Seismic velocity within the postrift unit varies significantly and is proportional to the carbonate content in the sediments. The structural style is defined by gentle conformable folds near the top, with faulting and complex halokinesis prevalent at the base.

3 FIRST LINE

The first section includes primarily subhorizontal interfaces and is about 9 km long. The depth of the water is close to 150 m, and both the subsidence and postrift units are approximately 2-km thick. Preprocessing steps included dip filtering and muting applied to CMP gathers to remove groundroll and some near-surface low-velocity dipping events; also, amplitudes at late times were boosted by a time-variant gain.

As the first step in building the velocity model, we identified the water bottom by migrating and stacking the data with a moveout velocity of 1500 m/s. Next, we estimated the velocity field of the underwater sediments. Because this layer is too thin ($\approx$ 400 m) to allow

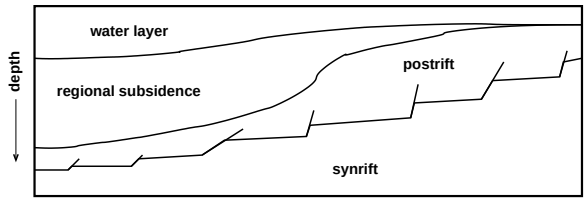

Figure 1. Cartoon of the geological history of the area depicting the subsidence, postrift, and synrift units.

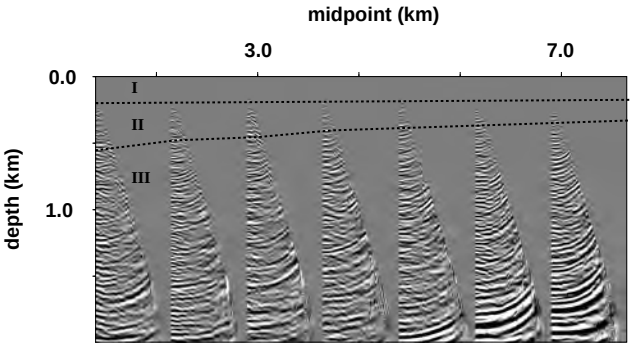

Figure 2. Common-image gathers (computed with an increment of 1 km) after Kirchhoff prestack depth migration with the velocity $V_{P0} = 1500$ m/s for the water and the parameters $V_{P0} = 1500$ m/s and $k_z = 0.8$ s^{-1} for the underwater sediments. Blocks I, II, and III used in the velocity analysis are separated by dashed lines that correspond to the deepest flat events within the first two blocks. The overcorrected events in block III indicate that the velocity field in block II is not appropriate for the deeper reflectors.

for picking of two events sufficiently separated in depth, we were unable to apply our MVA algorithm. Instead, we assumed that the underwater layer is isotropic with the water velocity (1500 m/s) at the top and computed the vertical gradient $k_z = 0.8$ s^{-1} using NMO velocities obtained from standard semblance velocity analysis. Figure 2 shows common-image gathers after migration with the estimated velocity field in the underwater layer (block II); the bottom of the layer is defined by the deepest events with no residual moveout.

Next, we apply migration velocity analysis to image gathers in block III. To get unique estimates of the medium parameters, we assumed that the vertical velocity V_{P0} is continuous at a certain point on the boundary between the second and the third blocks (see Paper II). Since the residual moveout of events in block III shows insignificant lateral variation (Figure 2), we expect that the lateral gradient k_x in this block can be neglected, and any point at the top of block III can be picked as the point of continuity. The velocity was taken to be continuous at the point ($x = 3000$ m, $z = 452$ m), which is

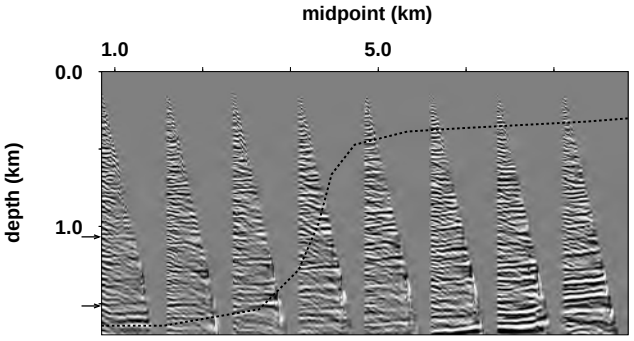

Figure 3. Common-image gathers after migration velocity analysis in block III (above the dashed line). The MVA operated with the two events marked by the arrows for midpoints between 1 km and 3 km. Most events below the dashed line exhibit residual moveout.

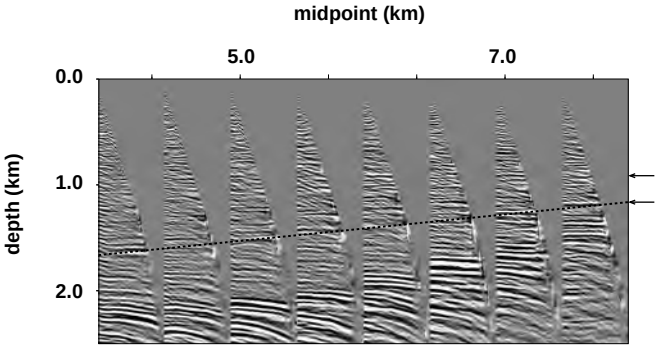

Figure 4. Common-image gathers after migration velocity analysis in block IV using the two events marked by the arrows for midpoints between 6.5 km and 8 km. The dashed line separates blocks III and IV, where events are practically flat, from the deeper part of the section.

close to the midpoints where we picked residual moveout and performed the MVA. Computing $V_{P0} = 1740$ m/s at the continuity point and minimizing the residual moveout of two events between midpoints 0 and 3 km (Figure 3), we estimated the parameters $k_z = 0.6 \pm 0.03$ s^{-1}, $k_x = 0.0 \pm 0.01$ s^{-1}, $\epsilon = 0.3 \pm 0.03$, and $\delta = 0.06 \pm 0.02$ in block III (see Paper II for a description of the error analysis). Note that the starting model for the MVA algorithm was isotropic and homogeneous.

The relatively large values of ϵ and δ, which yield $\eta = 0.21 \pm 0.03$, indicate that this block has pronounced anisotropy. While the inverted parameters remove residual moveout in image gathers at midpoints with coordinates less than 4 km, events in the right part of the section are overcorrected (Figure 3). Therefore, the third block has a limited lateral extent, as marked in Figure 3.

The results of MVA for block III indicate the need

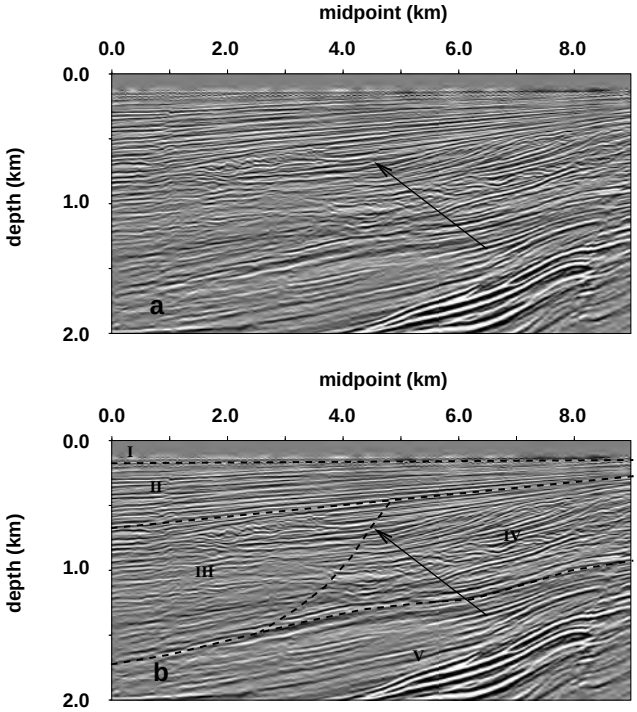

Figure 5. (a) First 2 km of the stacked depth section after prestack depth migration with the estimated parameters in blocks I–IV; (b) same section with delineated block boundaries. The arrow points to the fault that separates blocks III and IV.

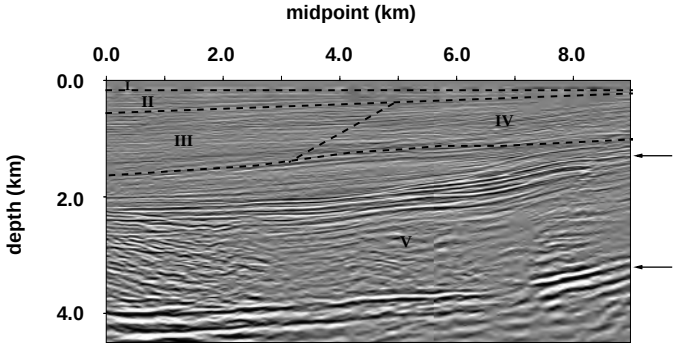

Figure 6. Stacked section after prestack depth migration with the estimated parameters in all five blocks. The arrows mark the events used in the velocity analysis for block V. The first (shallow) marked reflector is the bottom of the subsidence unit, and the second reflector is the bottom of the postrift unit. Note that the block boundaries of the velocity field do not follow the geological markers.

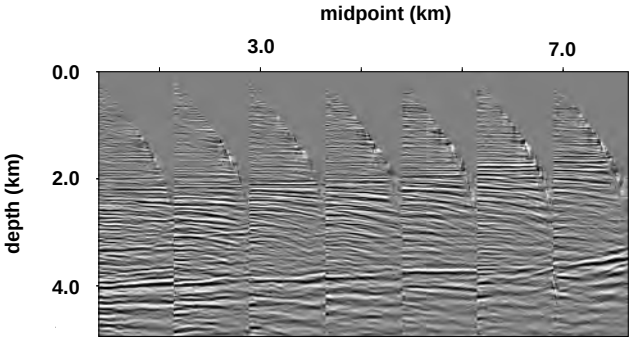

Figure 7. Common-image gathers after prestack depth migration with the estimated parameters. Most undercorrected events stack at extremely low velocities, and likely are interbed multiples.

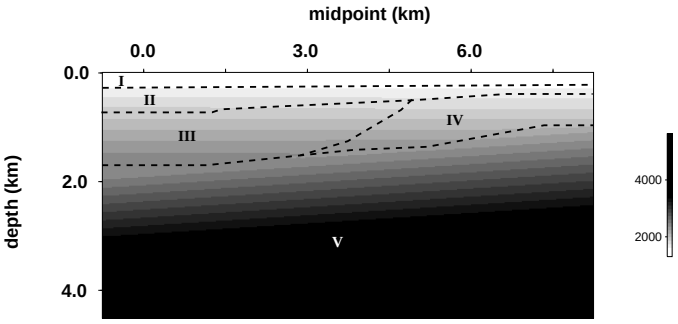

Figure 8. Depth section of the estimated vertical-velocity field. The dashed lines mark the block boundaries. The values in the legend are in m/s.

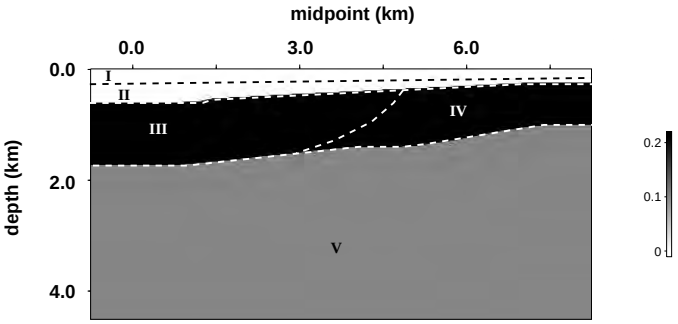

Figure 9. Depth section of the estimated anellipticity parameter η.

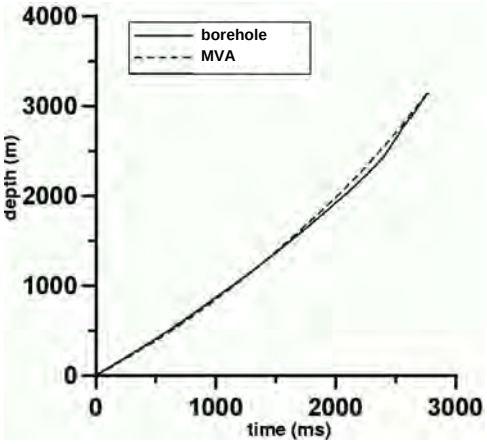

Figure 10. Comparison of the time-depth curves estimated from the MVA at midpoint 5 km (dashed) and derived from sonic logs and check-shot data in a borehole close to the seismic line (solid).

to introduce another block in the same depth interval but for midpoints to the right of the 4-km mark. Similar to the procedure described above, we selected the point of continuity between the underwater layer and the new block IV close to the midpoints where we performed the MVA ($x = 7000\,\mathrm{m}$, $z = 310$ m) and computed the vertical velocity at this point ($V_{P0} = 1625$ m/s). Keeping this value of V_{P0} fixed, we carried out the migration velocity analysis using the residual moveout of the two events marked in Figure 4 between midpoints 6 and 8 km. The algorithm converged to the following parameter estimates for block IV: $k_z = 0.65 \pm 0.03\ \mathrm{s}^{-1}$, $k_x = 0.0 \pm 0.01\ \mathrm{s}^{-1}$, $\epsilon = 0.35 \pm 0.03$, and $\delta = 0.1 \pm 0.02$. As illustrated by the stacked section in Figure 5, the boundary between the third and fourth blocks corresponds to a fault that stretches over a significant depth interval. While events in blocks III and IV (i.e., above the dashed line in Figure 4) are largely flat, and the shallow part of the image in Figure 5 exhibits good coherence and resolution, most deeper events remain undercorrected.

In contrast to that in the first four blocks, the residual moveout in the deeper part of the section (i.e., in block V) noticeably decreases to the right, which indicates a significant lateral velocity variation. To determine the point of velocity continuity at the top of block V in the presence of laterally varying velocity, we followed the procedure outined in Paper II. First, we performed prestack depth migration for a homogeneous isotropic medium using the vertical velocity at the bottom of block IV ($V_{P0} = 2230$ m/s). Since the minimum residual moveout in block V was observed at midpoint 7 km, the coordinates of the continuity point were found to be ($x = 7000\,\mathrm{m}, z = 1235\,\mathrm{m}$), where $V_{P0} = 2230$ m/s. Although this way of building a continuous velocity function relies on the assumption that the parameter

δ is small, it is acceptable for most practical situations (see Paper II).

Using the estimated vertical velocity at the top of block V, we obtained the rest of the parameters from the residual moveout along the two reflectors marked in Figure 6 for midpoints between 4 km and 6 km: $k_z = 0.83 \pm 0.04\ \mathrm{s}^{-1}$, $k_x = 0.04 \pm 0.01\ \mathrm{s}^{-1}$, $\epsilon = 0.19 \pm 0.03$, and $\delta = 0.06 \pm 0.03$. Figures 6 and Figure 7 display the final stacked image obtained after migration with the estimated parameters in all five blocks and the corresponding common-image gathers, most of which are practically flat.

The results of the velocity analysis are summarized in the depth sections of the vertical velocity and parameter η in Figures 8 and 9. As expected, the ubiquitous presence of shales in the subsidence unit at depths less than 2 km makes blocks III and IV strongly anisotropic, with values of η exceeding 0.2. The deeper postrift unit also exhibits non-negligible anisotropy and is characterized by moderate lateral velocity variation. In the subsidence unit, the maximum offset-to-depth ratio for the two reflectors used in the velocity analysis is close to two, which is large enough to provide sufficiently tight constraints on the parameter η. In the postrift unit, however, the maximum offset-to-depth ratio is suitable for evaluating η only for the shallow reflector. As a result, estimates of η for depths exceeding 2 km become unstable.

For this line, our maximum values of η exceed 0.2, which is larger than $\eta_{\max} \approx 0.1$ obtained by Alkhalifah (1996). Although this discrepancy seems to be quite significant, nonhyperbolic moveout inversion of horizontal events is known to be hampered by the tradeoff between η and the NMO velocity. As shown by Grechka and Tsvankin (1998) and Tsvankin (2001), the uncertainty in η estimates for offset-to-depth ratios of about two can reach ± 0.1. This instability in the inversion for η may have influenced our MVA technique and Alkhalifah's time-domain algorithm in different ways, in particular because the model assumptions in the two methods are not the same. Although Alkhalifah (1996) does not take lateral velocity variation into account, his method allows η to vary as a smooth function of the vertical time. In contrast, our MVA algorithm is designed to decouple anisotropy from vertical and lateral heterogeneity, but all anisotropic parameters are held constant within each factorized block.

On the whole, we believe that our estimates of η are more accurate, both because of the careful treatment of the spatial velocity variations and the higher stability of MVA (compared with time-domain techniques) in the presence of noise. The accuracy of our results is confirmed by the close match of the time-depth curve computed from our estimated vertical velocity with borehole data (Figure 10). We should keep in mind, however, the MVA method operating solely with P-wave data can reconstruct the vertical velocity in subhorizontal VTI layers only if the assumption about the continuity of V_{P0} across layer boundaries is correct (Paper II).

4 SECOND LINE

Although migration velocity analysis generally improves parameter estimation because of its robustness in the presence of noise, its main advantage over time-domain methods is in the ability to build laterally varying velocity fields. In this section, we apply our algorithm to another line from the same data set, where the anisotropy parameters and vertical velocity vary significantly in both vertical and horizontal directions. This line is further offshore and has a slightly deeper water column than does the first line. In addititon to the same preprocessing steps as those applied to the first line, the data were bandpass-filtered between 5 and 35 hz.

The final depth-migrated section and the factorized VTI blocks that comprise the model are shown in Figure 11. The medium parameters in each block (Figures 12–15) were estimated using the same procedure as that applied to the first line. For blocks II, III, IV, and V, the MVA was performed with a fixed value of the vertical velocity at the top of each block. We assumed that V_{P0} was continuous between blocks I and II, I and V, II and III, and II and IV. Since the vertical velocity in blocks I, II, III, and V is almost laterally invariant, the choice of this point of continuity was not important. For the fourth block, however, the lateral gradient k_x is substantial, and the continuity point was identified by applying homogeneous isotropic migration, as discussed above for the first line.

The maximum offset-to-depth ratio for most reflectors in block IV is less than two, which is insufficient for estimating the parameter η from nonhyperbolic moveout of subhorizontal events. To constrain η, we used reflections from the prominent fault plane with a dip of about 35° at the bottom of this block. Reflections from the shallow segment of the same dipping fault plane also provided important information for the parameter estimation in block III.

We had to ignore anisotropy in block VI because η could not be obtained from either nonhyperbolic moveout (the maximum offset-to-depth ratios were close to one) or dipping events. The velocity V_{P0} at the top of the block and the gradients k_z and k_x were estimated from the hyperbolic portion of the moveout curve for two reflectors sufficiently separated in depth.

The image gathers in Figure 16 demonstrate that the migration with the estimated model parameters flattens the majority of reflection events, which confirms that the piecewise factorized VTI medium is a good approximation for the velocity field in the area. The remaining residual moveout for several events is likely caused by multiples and velocity variations at a scale much smaller than the spread of a typical CMP gather.

Blocks II, III, IV, V, and the portion of block VI

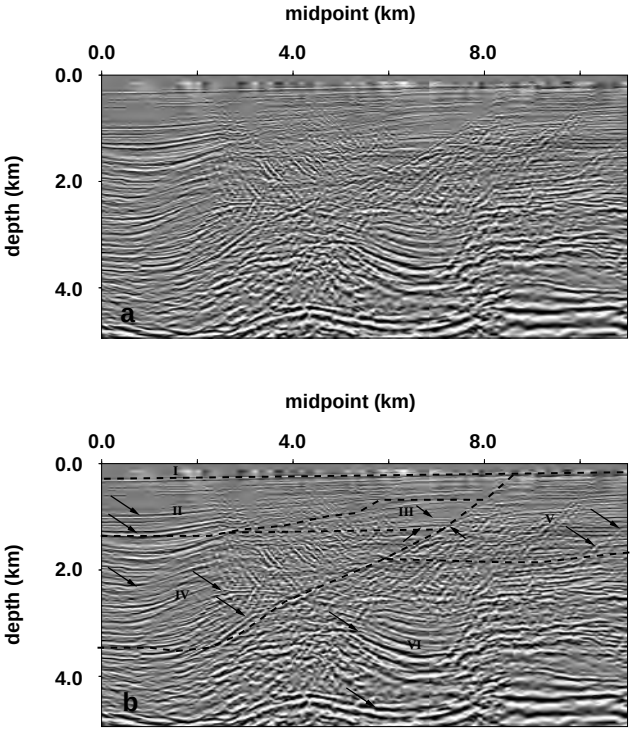

Figure 11. (a) Stacked section for the second line after prestack depth migration with the estimated parameters; (b) same section with delineated block boundaries. The arrows point to the reflectors used in the MVA. Block I is water with $V_{P0} = 1500$ m/s; the estimated parameters for block II are $V_{P0}(x = 4\,\text{km}, z = 240\,\text{m}) = 1500$ m/s, $k_z = 0.66 \pm 0.03$ s^{-1}, $k_x = 0.02 \pm 0.01$ s^{-1}, $\epsilon = 0.02 \pm 0.02$, and $\delta = -0.02 \pm 0.02$; for block III, $V_{P0}(x = 6.0\,\text{km}, z = 650\,\text{m}) = 1890$ m/s, $k_z = 0.4 \pm 0.04$ s^{-1}, $k_x = 0.01 \pm 0.01$ s^{-1}, $\epsilon = 0.12 \pm 0.03$, and $\delta = 0.03 \pm 0.03$; for block IV, $V_{P0}(x = 2.5\,\text{km}, z = 1400\,\text{m}) = 2200$ m/s, $k_z = 0.4 \pm 0.04$ s^{-1}, $k_x = -0.07 \pm 0.02$ s^{-1}, $\epsilon = 0.19 \pm 0.03$, and $\delta = 0.07 \pm 0.03$; for block V, $V_{P0}(x = 8.5\,\text{km}, z = 250\,\text{m}) = 1500$ m/s, $k_z = 0.65 \pm 0.03$ s^{-1}, $k_x = 0.03 \pm 0.02$ s^{-1}, $\epsilon = 0.15 \pm 0.02$, and $\delta = 0.06 \pm 0.02$; and for block VI, $V_{P0}(x = 6.5\,\text{km}, z = 1950\,\text{m}) = 2500$ m/s, $k_z = 0.65 \pm 0.03$ s^{-1}, $k_x = 0.16 \pm 0.02$ s^{-1}, $\epsilon = 0$, and $\delta = 0$.

above the first prominent reflector make up the subsidence unit, while the deeper part of the section belongs to the postrift unit. Blocks IV ($k_x = -0.07$ s^{-1}) and VI ($k_x = 0.16$ s^{-1}) exhibit significant lateral velocity variation, which results in a decrease in V_{P0} towards the middle of the section. Since this low-velocity zone is close to the major fault plane, it may point to a zone of weakness that often accompanies major faulting.

The magnitude of the parameter η for this line ($\eta_{\max} \approx 0.12 \pm 0.04$) is smaller than that for the first line. One possible reason for the lower η values is that the shales near the second line are less consolidated, and the clay platelets responsible for the effective anisotropy are not well aligned. The weaker anisotropy on the second

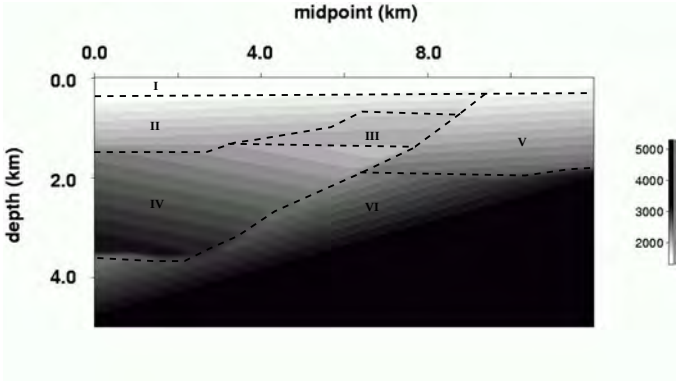

Figure 12. Depth section of the estimated vertical-velocity field. The values in the legend are in m/s.

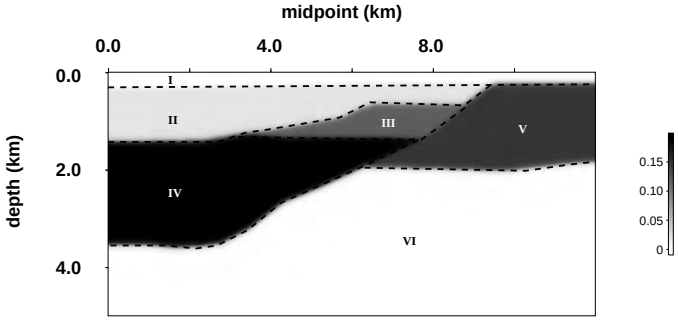

Figure 13. Depth section of the estimated parameter ϵ.

line can also be attributed to the influence of overpressure, which is well documented in this area (Brice et al., 1982; Alkhalifah, 1996). Overpressure may cause a reduction in the deviatoric stress, which, in turn, reduces the value of η (Sarkar et al., 2003). Although the magnitude of η is substantial only in blocks III, IV, and V, geological data indicate that the shales extend all the way to the bottom of the subsidence unit in block VI. Accurate estimation of η in block VI, however, requires larger offsets for subhorizontal events or more prominent dipping events.

Figure 17 was used by Alkhalifah (1996) and Alkhalifah et al. (1996) to illustrate the improvements in time imaging after taking anisotropy into account. For example, the anisotropic processing succeeded in imaging the fault plane at midpoint 7.5 km and depth 3 km (Figure 17b), which is absent on the isotropic image (Figure 17a). Also, the major fault plane that runs through the section between midpoints 2 and 8 km and subhorizontal reflectors near midpoint 3 km and depth 2.7 km show improved continuity on the anisotropic section.

Comparison of the prestack depth-migrated image in Figure 18b and the time-migrated image in Figure 18a

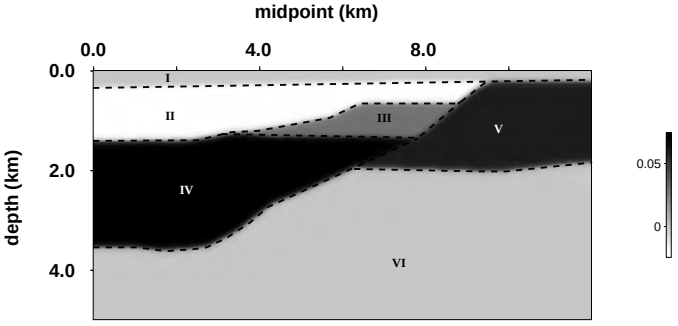

Figure 14. Depth section of the estimated parameter δ.

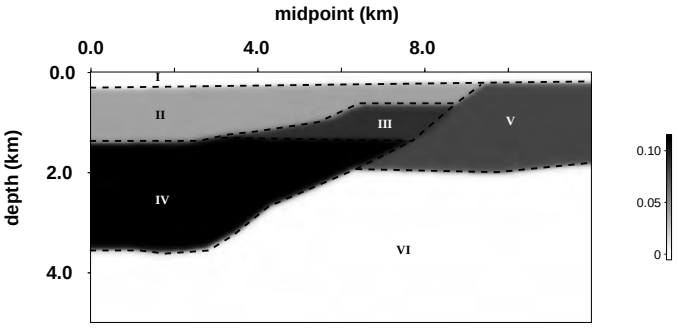

Figure 15. Depth section of the estimated parameter η.

illustrates further improvements achieved by the MVA and prestack depth migration. Better focusing and continuity are observed for the major fault plane between midpoints 2 and 8 km and several reflectors just above and below it, for the subhorizontal reflectors at midpoint 4.5 km and depth 1.4 km, and for the fault plane at midpoint 7.5 km and depth 3 km. Since time migration ignores the lateral velocity variation in block IV, the antithetic faults, which are clearly visible at midpoint 4 km and depth 2 km on the depth-migrated section, appear fuzzy in Figure 18a.

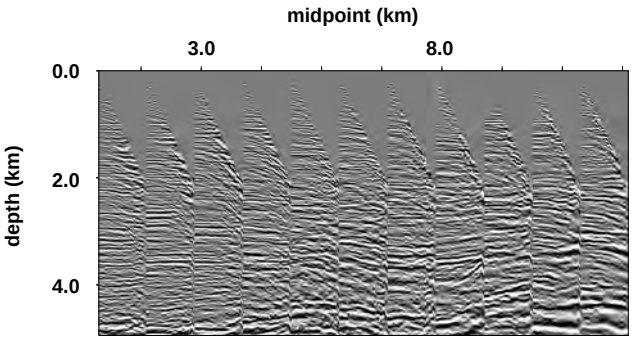

Figure 16. Common-image gathers (at 1-km spacing) after migration with the estimated parameters.

Perhaps the most dramatic difference between the two images is in the shape and position of the two prominent reflectors that define the top and bottom of the postrift unit (between depths 2.5 and 5 km) and span the entire lateral extent of the section. Because time migration does not account for the lateral variation in the vertical velocity, these two reflectors appear dipping on the time-migrated image. This dip was largely removed in Figure 18b by taking into account the significant lateral velocity variation in block VI.

As was the case for the first line, our estimates of the maximum value of η ($\eta_{\max} \approx 0.12$) are somewhat different from those reported by Alkhalifah (1996) and Alkhalifah et al. (1996) ($\eta_{\max} \approx 0.2$). We believe that the main reason for this discrepancy is the presence of significant lateral heterogeneity in blocks IV and VI, which was not taken into account in the DMO-based inversion method of Alkhalifah (1996). The high image quality in Figure 18b indicates that the application of our MVA method helped to describe the spatial velocity variation with greater resolution and accuracy compared to those for the time-domain techniques.

5 DISCUSSION AND CONCLUSIONS

By approximating the subsurface with factorized $v(x, z)$ VTI media, it is possible to properly account for both vertical and lateral variation in the anisotropic velocity field. Here, we applied to field data a migration velocity-analysis method designed for VTI models composed of factorized layers or blocks. This MVA algorithm, introduced in Sarkar and Tsvankin (2004; Paper II) has two important new features that distinguish it from conventional velocity-analysis techniques:

(1) since estimation of the anisotropic coefficient η typically requires nonhyperbolic (long-spread) moveout information, we implemented a two-parameter semblance scan on image gathers to evaluate both hyperbolic and nonhyperbolic parts of the residual moveout function. When the semblance operator fails because of substantial amplitude variation with offset, as may happen in the presence of polarity reversals in Class II sands, modified semblance routines suggested by Sarkar et al. (2001, 2002) may be used instead.

(2) evaluation of the vertical and lateral velocity gradients in each block is accomplished by minimizing residual moveout along at least two reflectors sufficiently separated in depth.

Application of our MVA method to offshore data from West Africa confirms the results of previous studies (Ball, 1995; Alkhalifah, 1996; Alkhalifah et al., 1996; Toldi et al., 1999) that massive shales in that area are strongly anisotropic, with the parameter η on one of

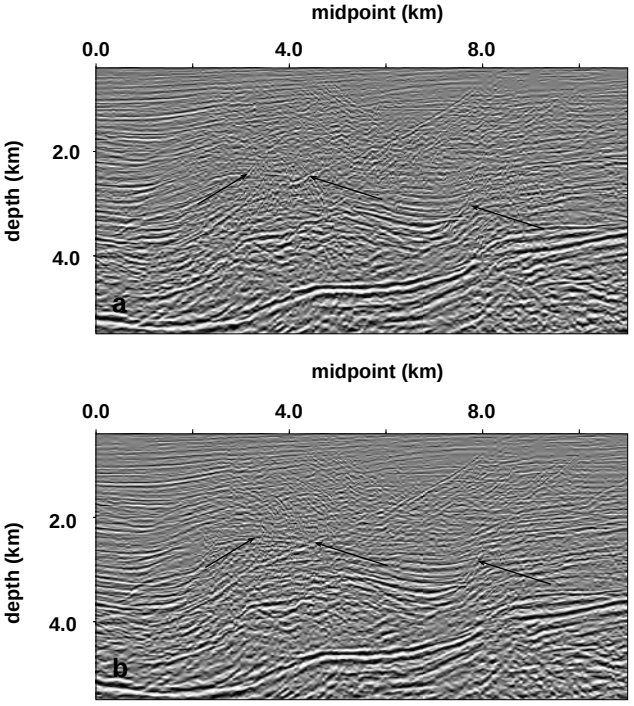

Figure 17. Second section after (a) isotropic and (b) anisotropic phase-shift time migration (from Alkhalifah et al., 1996). Both sections were filtered to match the amplitude spectrum of the depth-migrated section in Figure 11 and stretched to depth using the vertical-velocity function from Figure 12. The arrows point to the main improvements achieved by taking anisotropy into account.

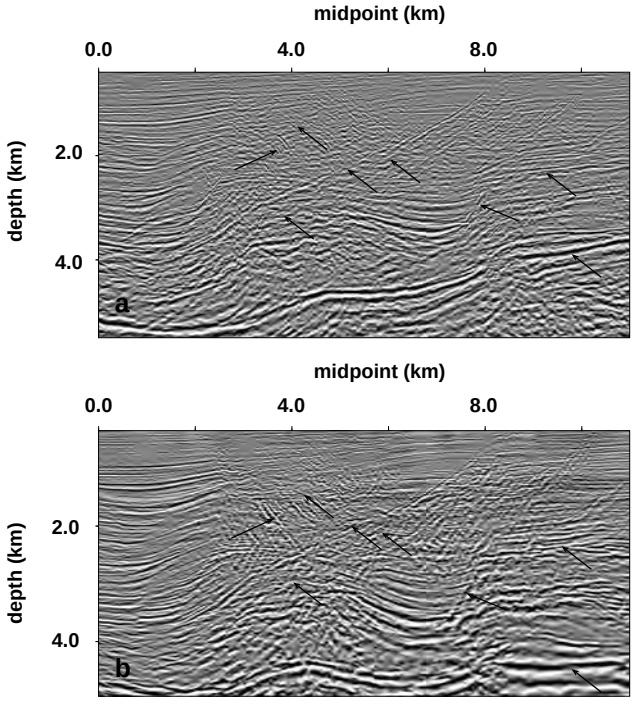

Figure 18. Second section after (a) anisotropic phase-shift time migration (Figure 17b) and (b) prestack depth migration (Figure 11). The arrows point to the main improvements achieved by applying the MVA and prestack depth migration.

the lines exceeding 0.2. The reconstructed velocity field also indicates the presence of substantial lateral heterogeneity in some of the layers, which was unaccounted for by the time-domain techniques of Alkhalifah et al. (1996) and Toldi et al. (1999). Since the piecewise factorized VTI model can handle both anisotropy and heterogeneity, our MVA algorithm produced more accurate estimates of the anisotropic coefficients than those obtained previously in the time domain by inverting dip moveout or long-spread traveltimes of horizontal events.

Anisotropic prestack depth migration with the reconstructed velocity field resulted in a number of significant improvements in image quality compared to the time sections of Alkhalifah et al. (1996). In particular, most faults on the depth-migrated image show greater continuity, the antithetic faults that are fuzzy on the time images are well focused, and subhorizontal reflectors within the anisotropic layers are better positioned and stacked. The accurate depth scale of our velocity model substantially changed the structure of the deeper part of one of the sections, where false dips seen on the time-migrated image were removed after the MVA and prestack depth migration.

Flat image gathers after the iterative maigration velocity analysis suggest that the factorized $v(x,z)$ VTI medium provides an adequate approximation for realistic, spatially varying anisotropic velocity fields. Although the vertical velocity can seldom be constrained by P-wave reflection data alone, the field-data example discussed here indicates that the assumption of a continuous vertical velocity field offers a practical way to build anisotropic models for prestack depth migration with minimal *a priori* information. Furthermore, as confirmed by this case study, in the absence of pronounced velocity jumps across medium interfaces, the time-depth curve obtained from the MVA algorithm closely matches the curve computed from borehole data.

Similar to any other MVA technique, the main cost of our method is in the repeated application of prestack migration, which makes this algorithm substantially more expensive than the time-domain parameter-estimation methods of Alkhalifah and Tsvankin (1995), Alkhalifah et al. (1996), and Grechka et al. (2002). The time-domain algorithms, however, produce inferior results in the presence of lateral velocity variation, as illustrated by the examples above.

Although migration becomes somewhat more time-consuming in the presence of anisotropy because of the

need to use anisotropic ray tracing, this extra cost is insignificant in comparison with the computing time for the actual migration step, which does not change for anisotropic media. Still, because of the larger number of the medium parameters, including anisotropy in MVA leads to a slower convergence towards the best-fit model. These additional MVA and migration steps make our algorithm more time-consuming than comparable isotropic techniques.

6 ACKNOWLEDGMENTS

We are grateful to Greg Ball and John Toldi of Chevron-Texaco for numerous helpful suggestions and for making the data available to CWP. We would like to thank members of the A(nisotropy)-Team of the Center for Wave Phenomena (CWP), Colorado School of Mines, for useful discussions and Ken Larner (CSM) for his review of the manuscript. The support for this work was provided by the Consortium Project on Seismic Inverse Methods for Complex Structures at CWP and by the Chemical Sciences, Geosciences and Biosciences Division, Office of Basic Energy Sciences, U.S. Department of Energy.

REFERENCES

Alkhalifah, T., 1996, Velocity analysis for transversely isotropic media: PhD thesis, Colorado School of Mines.

Alkhalifah, T., 1997, Seismic data processing in vertically inhomogeneous TI media: Geophysics, **62**, 662–675.

Alkhalifah, T., and Tsvankin, I., 1995, Velocity analysis for transversely isotropic media: Geophysics, **60**, 1550–1566.

Alkhalifah, T., Tsvankin, I., Larner, K. and Toldi, J., 1996, Velocity analysis and imaging in transversely isotropic media: Methodology and a case study: The Leading Edge, **15**, 371–378.

Ball, G., 1995, Estimation of anisotropy and anisotropic 3-D prestack migration, offshore Zaire: Geophysics, **60**, 1495–1513.

Brice, S. R., Cochran, M. D., Pardo, G., and Edwards, A. D., 1982, Tectonics and sedimentation of the South Atlantic rift sequence: Cabinda, Angola: Studies in continental margin geology, AAPG memoir, **34**, J. S. Watkins and C. L. Drake Eds.

Chauris, H., and Noble, M., 2001, Two-dimensional velocity macro model estimation from seismic reflection data by local differential semblance optimization: Application to synthetic and real datasets, Geophys. J. Int., **144**, 14–26.

Faust, L. Y., 1951, Seismic velocity as a function of depth and geologic time: Geophysics, **16**, 192–206.

Faust, L. Y., 1953, A velocity function including lithologic variation: Geophysics, **18**, 271–288.

Gardner, G.H.F., French, W.S., and Matzuk, T., 1974, Elements of migration and velocity analysis: Geophysics, **39**, 811–825.

Grechka, V., and Tsvankin, I., 1998, Feasibility of nonhyperbolic moveout inversion in transversely isotropic media: Geophysics, **63**, 957–969.

Grechka, V., Pech, A., and Tsvankin, I., 2002, P-wave stacking-velocity tomography for VTI media: Geophys. Prosp., **50**, 151–168.

Han, B., Galikeev, T., Grechka, V., Le Rousseau, J., and Tsvankin, I., 2000, A synthetic example of anisotropic P-wave processing for a model from the Gulf of Mexico, *in* Ikelle, L., and Gangi, A., Eds., Anisotropy 2000: Fractures, converted waves and case studies: Proceedings of the Ninth International Workshop on Seismic Anisotropy (9IWSA), Soc. Expl. Geophys.

Liu, Z., 1997, An analytical approach to migration velocity analysis: Geophysics, **62**, 1238–1249.

Sarkar, D., Castagna, J. P., and Lamb, W., 2001, AVO and velocity analysis: Geophysics, **66**, 1284–1294.

Sarkar, D., Baumel, R. T., Larner, K., 2002, Velocity analysis in the presence of amplitude variation: Geophysics, **67**, 1664–1672.

Sarkar, D., Bakulin, A., Kranz, R. L., 2003, Anisotropic inversion of seismic data for stressed media: Theory and a physical modeling study on Berea Sandstone: Geophysics, **68**, 690–704.

Sarkar, D., and Tsvankin, I., 2003, Analysis of image gathers in factorized VTI media: Geophysics, **68**, 2016–2025.

Sarkar, D., and Tsvankin, I., 2004, Migration velocity analysis in factorized VTI media: Geophysics, in print.

Stork, C., 1992, Reflection tomography in the post migrated domain: Geophysics, **57**, 680–692.

Thomsen, L., 1986, Weak elastic anisotropy: Geophysics, **51**, 1954–1966.

Toldi, J., Alkhalifah, T., Berthet, P., Arnaud, J., Williamson, P., and Conche, B., 1999, Case study of estimation of anisotropy: The Leading Edge, **18**, no. 5, 588–594.

Tsvankin, I., 2001, Seismic signatures and analysis of reflection data in anisotropic media: Elsevier Science Publ. Co., Inc.

APPENDIX A: MVA IN THE PRESENCE OF NONLINEAR VELOCITY VARIATION

The purpose of this appendix is to evaluate the distortions produced by our MVA algorithm when the vertical velocity is a *nonlinear* function of depth z. Consider a factorized VTI medium with the vertical velocity defined as $V_{P0}(z) = V_{P0} + A\,z^2$, and assume that reflection moveout was recorded from eight horizontal interfaces at depth intervals of 500 m.

To reconstruct the vertical velocity variation, we approximated the subsurface with three horizontal factorized $v(z)$ layers marked in Figure A1a. Using the

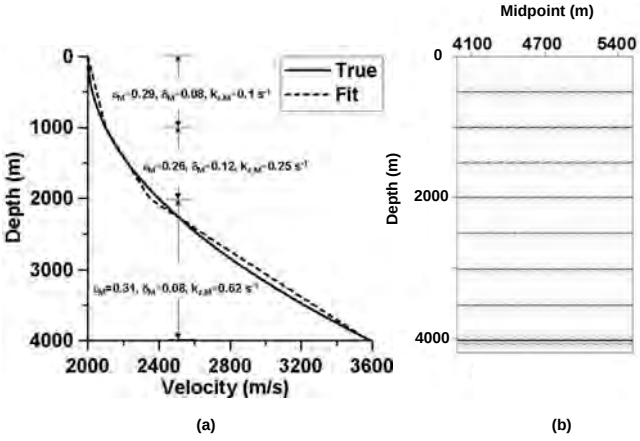

Figure A1. (a) Comparison of the true (solid line) and estimated (dashed line) vertical velocity V_{P0} for a VTI medium with $V_{P0}(z) = 2000 + 0.0001z^2$ (z is in meters, V_{P0} is in m/s), $\epsilon = 0.3$, and $\delta = 0.1$. The migration velocity analysis was performed for three factorized $v(z)$ layers with the boundaries marked on the plot. The reflectors are spaced every 500 m, and the maximum offset is equal to 4000 m. The interval parameters (subscript "M") were estimated using the moveout associated with two reflectors in each factorized layer. (b) Image gathers obtained after prestack depth migration with the estimated parameters shown on plot (a).

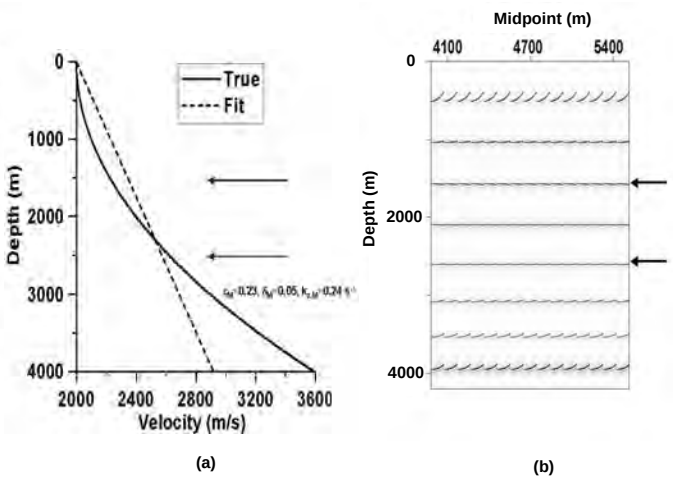

Figure A2. Same as Figure A1, but the MVA was performed for a single factorized $v(z)$ layer using the moveout associated with the reflectors at depths 1500 and 2500 m (marked by the arrows).

moveout associated with two reflectors for each factorized $v(z)$ layer, we obtained a piecewise factorized medium with the function $V_{P0}(z)$ that closely reproduces the true nonlinear vertical-velocity variation (Figure A1a). The vertical velocity at the top of the model was fixed at the correct value, while the velocities in the two deeper layers were found under the assumption that V_{P0} is a continuous function of depth. The accuracy of the estimated three-layer factorized model is confirmed by the flat image gathers in Figure A1b.

The success of the piecewise-linear velocity approximation, however, depends on whether the available reflectors sample the velocity function in sufficient detail. Consider the same true medium as that in Figure A1, but now with only two reflectors (located at depths of 1500 m and 2500 m) available for velocity analysis. In this case, our MVA algorithm can estimate the parameters of just one factorized $v(z)$ layer (Figure A2a). As illustrated by the image gathers in Figure A2b, the events associated with the reflectors used in the velocity analysis are flat. Events both above 1500 m and below 2500 m, however, are overcorrected because the NMO velocities for them are too low. Clearly, no single factorized medium can properly image reflection events for the whole range of depths.